Chemical Science

ROYAL SOCIETY OF CHEMISTRY

EDGE ARTICLE

View Article Online
View Journal | View Issue

Cite this: *Chem. Sci.*, 2023, **14**, 8497

All publication charges for this article have been paid for by the Royal Society of Chemistry

Push-pull photochromic dyes for semi-transparent solar cells with light-adjustable optical properties and high color-rendering index†

Samuel Fauvel,[a] Antonio J. Riquelme,[a] José-María Andrés Castán,[a] Valid Mwatati Mwalukuku,[a] Yann Kervella,[a] Vijay Kumar Challuri ,[b] Frédéric Sauvage, [c] Stéphanie Narbey,[d] Pascale Maldivi, [a] Cyril Aumaître [a] and Renaud Demadrille *[a]

Received 7th May 2023
Accepted 10th July 2023

DOI: 10.1039/d3sc02328a

rsc.li/chemical-science

We report the design, synthesis and characterization of push–pull photochromic naphthopyran dyes, incorporating different carbazole moieties as the electron-donor group for use in dye-sensitized solar cells. Compared to a reference dye incorporating a diphenylamine-type donor moiety, the introduction of functionalized carbazoles allows for a hypsochromic shift of the absorption of the coloured isomers of the dyes in the visible region and a better tuning of their spectra to the photopic response of the human eye. Under illumination, the molecules exhibit a broad absorption with a maximum comprised between 546 nm and 571 nm in solution and they reveal relatively fast discoloration kinetics. By using these dyes to fabricate photochromic solar cells whose optical and photovoltaic properties vary with the light exposure, we have achieved a PCE of up to 3% in opaque cells. Using these molecules in semi-transparent solar cells with different electrolytes, a PCE of 2.3% was achieved. We also produced a semi-transparent mini-module with an average visible transmittance varying between 66% and 50% and a colour rendering index around 95 in both the uncoloured and coloured states.

Introduction

Since the 1990's, the efforts to develop alternative photovoltaic (PV) technologies to silicon have been steadily increasing.[1,2] The emergence of solar cells integrating fully organic or hybrid materials in the photoactive layer,[3,4] and more recently the development of semi-transparent devices[5,6] have opened up new prospects for PV applications in IoT[7,8] (Internet of Things) devices, buildings,[9–12] vehicles[13] and greenhouses.[14,15] Among these technologies, Dye-Sensitized Solar cells (DSSCs) are attractive because they combine many advantages.[16] First, today their power conversion efficiencies (PCE) have now reached 15% under standard irradiation conditions[17] and over 36% under low light conditions.[18] Second, when non-volatile electrolytes are used, their stability is greatly improved and lifetimes in excess of 10 years have already been demonstrated in accelerated ageing tests,[19] and reaching 12 years in real-world.[20] Thirdly, these solar cells and the corresponding modules are fully customizable;[2,21,22] their shape, colour, and transparency can be adjusted during the manufacturing process.[23] Finally, their energy payback time[24] and carbon footprint are estimated to be lower than for silicon-based solar cells. In 2020, we introduced in the field a new class of multifunctional DSSCs based on photochromic dyes.[25] Because of their optical response to a light stimulus, photochromic dyes can be used in a wide range of applications, such as data storage,[26] actuators,[27] sensing,[28,29] optical lenses[30] or bio-imaging,[31,32] but their study in photovoltaics is recent.[33–35] Using the classic donor-π-conjugated-bridge-acceptor structure for the dyes where the π-conjugated bridge is replaced by a photochromic moiety, we have obtained DSSCs that can change colour and self-adjust their light transmittance upon exposure to sunlight. In 2023, we explored this concept and showed that photochromic solar cells can achieve a PCE of over 4.3% in the opaque configuration and a PCE of up to 3.9% in the semi-transparent configuration.[36] Molecular engineering of the dyes allowed us to improve the photochromic behaviour of the devices and the best photochromic solar cells exhibited a reversible change in average visible transmittance (AVT) of about 40% between the uncoloured and coloured states. These performances have been obtained with a push–pull compound of the diphenylnaphthopyran family containing a diphenylamine group as an

[a]*Université Grenoble Alpes, CEA, CNRS, IRIG-SyMMES, F-38000 Grenoble, France. E-mail: renaud.demadrille@cea.fr*

[b]*G-Lyte, Hub de l'énergie, 15 Rue Baudelocque, 80039 Amiens, France*

[c]*Laboratoire de Réactivité et Chimie des Solides, CNRS UMR7314, Université de Picardie Jules Verne, Hub de l'énergie, 15 Rue Baudelocque, 80039 Amiens, France*

[d]*Solaronix SA, Rue de l'Ouriette 129, 1170 Aubonne, Switzerland*

† Electronic supplementary information (ESI) available: Synthesis procedures, characterization techniques, solar cells fabrication. See DOI: https://doi.org/10.1039/d3sc02328a

electron donor. The strong electron-donating effect induced by the diphenylamine moiety in these push–pull dyes gives a green tint to the cells under irradiation resulting in a colour-rendering index (CRI) for semi-transparent devices of around 65. In general, a CRI of 80 or higher is desired for glazing applications, and ideally the CRI should be greater than 90.[13] Therefore, in order to use these solar cells for building or vehicle integrated photovoltaics, it is important to improve their CRI.[37,38] To solve this problem, in this work we are interested in modulating the push–pull effect in diphenyl-naphthopyran dyes in order to obtain photochromic molecules whose absorption in the coloured state better matches the photopic vision of the human eye which allows colour perception. To this end, we have developed a series of five compounds in which the electron-donating moiety is a carbazole unit[39,40] whose donating strength is modulated by substitution. After their synthesis, the photochromic and optoelectronic properties of the dyes were investigated before their use in the fabrication of opaque and semi-transparent DSSCs. We show that by replacing the diphenylamine group with modified carbazole units, the optical properties of the dyes can be tuned to better match the photopic response of the human eye. The new compounds have a maximum absorption wavelength between 546 nm and 571 nm, close to the maximum photopic response of the human eye at 555 nm. In addition, the use of carbazole units allows the HOMO energy level of the dyes to be lowered, opening the way for the use of redox systems other than tri-iodide/iodide-based electrolytes. We, therefore, present the first photochromic cells based on a cobalt-based or the recently developed transparent hybrid sulfurothioate-based redox system.[41] We found that some of the dyes show a maximum PCE of about 3% in opaque cells and 2.3% in transparent devices. We also report a transparent solar mini-module that shows light-dependent AVT, varying between 66% and 50% and a CRI above 96 in the non-activated state, which remains above 95 after colouring of the cells.

Results and discussion

Synthesis of the push-pull photochromic dyes

To investigate the effect of the electron-donating strength of the carbazole moiety on the photochromic and optoelectronic properties of the dyes, we designed different carbazole precursors by varying the substituents at positions 3 and 6, as shown in Fig. 1. We also selected two commercial carbazole derivatives **C1** and **C4**, purchased from Sigma Aldrich and Ikamba Organics respectively.[42] The carbazole **C2** containing two 4-octylthiophene units was obtained by Suzuki–Miyaura coupling from 3,6-dibromo-carbazole and 5-*n*-octylthiophene-2-boronic acid. For the carbazole **C3**, we started with the alkylation of bromoresorcinol before using it in a similar reaction. For the synthesis of the **C5** carbazole, we protected the nitrogen of the 3,6-dibromocarbazole to prevent a polymerisation reaction during the Buchwald–Hartwig coupling. The compound **C5** was obtained by the same reaction starting with di(hexyloxy)-diphenylamine. The dyes were then synthesized as described in Fig. 1. First, the protected naphthol **P3** was prepared as described in ESI.† The different carbazole precursors were coupled to this naphthol *via* a Buchwald–Hartwig reaction and the resulting naphthols were deprotected *in situ*. The deprotected naphthols **X1-5** were then subjected to a chromenisation reaction with the acetal-protected propargyl alcohol **A5** to give the photochromic intermediates **Y1-5**. The final **SF1-5** dyes were obtained by Knoevenagel condensation with cyano-acrylic acid.

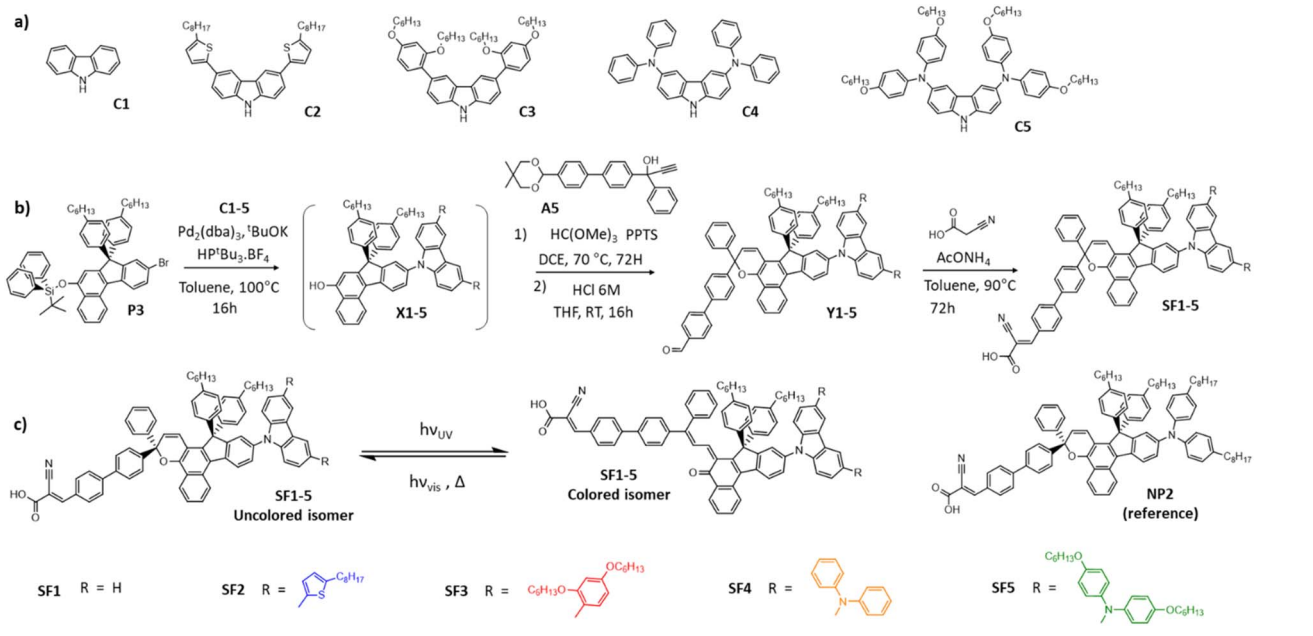

Fig. 1 a) Chemical structures of the carbazole donor units (**C1-5**) used in this work. (b) Synthetic route towards the dyes **SF1-5**. (c) General photochromic interconversion mechanism for the dyes **SF1-5** and structure of the **NP2** molecule used as a reference.

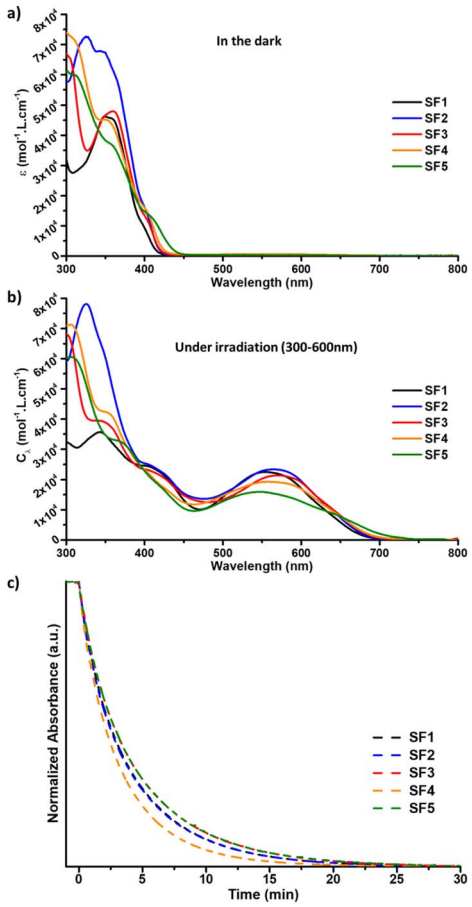

Fig. 2 UV-visible absorption spectrum for **SF1**, **SF2**, **SF3**, **SF4** and **SF5** without (a) and with (b) under continuous irradiation (Xenon lamp, 200 W, 300–600 nm, orthogonal with respect to the measuring beam). Concentration: 2×10^{-5} mol L^{-1} in toluene at 25 °C. (c) Comparison of normalized discoloration curves of **SF1-5** in solution after reaching PSS. Concentration: 2×10^{-5} mol L^{-1} in toluene at 25 °C.

Fig. 1 also shows the photochromic interconversion reaction between the closed (uncoloured) and open form (coloured) isomers and the structure of the dye **NP2**, which was used as a reference molecule in this work.

Optical and photochromic properties of the dyes in solution

The photochromic behaviour and optical properties of the dyes were studied by UV-vis spectroscopy in toluene solution according to a classical method.[43,44] The spectra were recorded in the dark and under illumination with a polychromatic light source from long to short wavelengths to avoid any interference from the measurement technique (*i.e.* conversion of the dyes from the close to the open form with UV photons during the measurement). The results were compared with data obtained from **NP2**, a photochromic dye used as a reference.[25] **NP2** is a diphenyl-naphthopyran dye containing a diphenylamine as a donor unit and produces the highest PCE ever recorded for a photochromic dye in DSSCs.

The absorption spectra of the closed and open form isomers of **SF1-5** are shown and compared in Fig. 2 and their optical parameters are summarized in Table 1 (see also ESI†). The absorption spectra of the dyes recorded in the dark and shown in Fig. 2a show absorption bands between 300 nm and 400 nm corresponding to π–π* transitions. The absorption limit of the closed isomers is between 416 nm and 440 nm depending on the structure of the donor moiety. These values are lower compared to **NP2** dye, whose absorption tail reaches 450 nm. The weakest absorption is observed for the **SF1** dye containing a bare carbazole unit, while the strongest absorption is observed for the **SF2** dye based on a carbazole moiety substituted with two octylthiophenes.

Fig. 2b shows the absorption spectra of the dyes recorded under illumination. In this family of dyes, absorption of a UV-photon leads to the cleavage of the carbon–oxygen bond of the pyran ring and rearrangement of the pi-conjugated system.[45] In the naphthopyran series, homolytic cleavage is usually reported as the main process for C–O bond dissociation.[44,46] Photogenerated open-form (OF) isomers exhibit increased delocalisation of the pi-electrons, resulting in the extension of the absorption spectrum into the visible region. Two types of transitions are observed. The band or shoulder located between 400 and 460 nm corresponds to new π–π* transitions. The second absorption band, which appears at longer wavelengths, corresponds to a mix of internal charge transfer (ICT) transitions occurring between the donor unit and the core of the

Table 1 Optical and photochromic parameters of the dyes **SF1-5**

	Optical properties					Electronic properties		
	λ_{max}[a] nm	C_λ[a] L mol^{-1} cm^{-1}	$k_{closing}$[b] $\times 10^{-3}$ s^{-1}	λ_{onset}[c] nm	ΔE_{opt}[c,d] eV	HOMO[e] eV	LUMO[e] eV	ΔE_{elec}[e,f] eV
NP2	620	19 000	2.30	730 (450)	1.70 (2.76)	−5.0 (−4.9)	−3.8 (−3.3)	1.2 (1.6)
SF1	554	22 500	4.14	675 (416)	1.84 (2.98)	−5.6 (−5.4)	−3.8 (−3.3)	1.8 (2.1)
SF2	565	23 400	4.22	681 (421)	1.82 (2.95)	−5.5 (−5.2)	−3.9 (−3.3)	1.6 (1.9)
SF3	571	21 400	3.72	687 (418)	1.80 (2.97)	−5.5 (−5.3)	−3.9 (−3.3)	1.6 (2.0)
SF4	557	19 300	4.96	692 (424)	1.79 (2.92)	−5.2 (−5.0)	−3.8 (−3.3)	1.4 (1.7)
SF5	546	15 900	3.75	717 (439)	1.73 (2.82)	−5.0 (−4.9)	−3.9 (−3.3)	1.1 (1.6)

[a] Obtained from the UV-visible spectra of the open form of the dyes. [b] Calculated from the decrease of absorption at the λ_{max} of the open form of the dyes at 25 °C. [c] Obtained from the UV-visible spectra of the open form of the dyes. Parenthesis, obtained from the close form. [d] Calculated from the optical absorption onset. [e] Values calculated from oxidation potential for the HOMO and electronic affinity for the LUMO, measured by CV in dichloromethane (DCM) (2×10^{-3} mol L^{-1}) at room temperature, Fc/Fc^+ was used as the internal standard. Parenthesis, determined by DFT calculations. [f] $\Delta E_{elec} = E_{LUMO} - E_{HOMO}$.

molecule or the photochromic core and the diene system extending to the anchoring function as demonstrated by TD-DFT calculations (see ESI†). The λ_{max} of the OF isomers is between 546 nm and 571 nm for all dyes, which is close to the maximum photopic response of the human eye. The λ_{onset} and optical band gap values for the open isomers vary with the electron donor strength of the carbazole moiety. The absorption region for the new series of dyes is blue-shifted compared to that of **NP2**, which has a λ_{max} located at 620 nm and an absorption limit at 730 nm. This hypsochromic shift of the ICT band is a direct consequence of the weaker electron-donating strength of the carbazole units compared to the diphenylamine. This is probably due to the high twist angle observed by DFT between the carbazole unit and the photochromic core, *e.g.* 51.2° in **SF1**. In the **NP2** molecule, the twist angle between the diphenylamine and the photochromic unit is only 2°. Under illumination, we found that a stabilization time of 180 seconds is sufficient to reach the photo-stationary state (PSS). The photostationary state corresponds to the equilibrium between the closed and open isomers. This equilibrium is reached under irradiation at a given temperature. Note that the solutions were kept at 25 °C with stirring to ensure accurate measurements. From the absorption in the PSS, the colourability C_λ of the dye is calculated. This value is the maximum absorption achieved by the dye in the visible range under illumination, divided by its concentration in solution. From the PSS, we can also determine the ring closure kinetic constants by following the bleaching of the solution in the dark at the maximum absorption wavelength. The values of these photochromic parameters are shown in Table 1. If we look at the colourability values, they all fall in the same range, between 15 900 and 23 400 L mol^{-1} cm^{-1}, and are quite comparable to those of the **NP2** dye (19 000 L mol^{-1} cm^{-1}). This suggests that the colourability of these molecules is related to the nature of the diphenyl-naphthopyran core and is relatively unaffected by substitution in that position.

The values of the discoloration kinetic constant k were obtained by fitting the fading curves with a mono-exponential equation[36] (see ESI†). For the **SF1-5** dyes the k values are all comprised between 3.72×10^{-3} s^{-1} and 4.96×10^{-3} s^{-1} and are higher than those of **NP2**, which contains a diphenylamine donating group. This observation confirms previous studies, which have shown that the introduction of electron-donor groups in the diphenyl-naphthopyran series helps to control the stability of open form isomers and the rate of discoloration.[47,48] Solutions containing our new dyes recover 80% of their original transparency in less than 8 minutes, and this time drops to 5 minutes for solutions based on **SF4**. This property is particularly interesting for a transparent solar cell application, although the kinetics are generally slower in complete device due to immobilisation of the dye on the electrode and interactions with the electrolyte.

Energy levels of dyes in their different states

For the use of these new dyes in DSSC-type devices, it is essential to ensure that their HOMO–LUMO energy levels in their different states are compatible with the energy level of the TiO_2 conduction band and the redox potential of the mediator used in the electrolyte.[16]

The energy levels of the frontier orbitals were determined by cyclic voltammetry. The measurements were performed in anhydrous DCM with 0.1 mol L^{-1} $TBAPF_6$ as supporting electrolyte, a silver electrode in 0.01 mol L^{-1} $AgNO_3$ solution as a reference, Fc^+/Fc as internal reference and the dye concentration was set to 2×10^{-3} mol L^{-1}. To study the energy levels of the dyes in their activated and non-activated states, measurements were performed in the dark and under irradiation. To determine the oxidation and reduction potentials of the open form isomers, the solutions were cooled in an ice bath to reduce the ring closure kinetics of the open form species and exposed to light to reach a higher concentration of coloured isomers at the PSS (more information related to these experiments can be found in ESI†). Fig. 3 is a diagram showing the energy levels obtained experimentally and from theoretical modelling using DFT with the B3LYP/TZ2P hybrid functional for the five carbazole dyes together with the energy levels of TiO_2 and the redox mediators I^-/I_3^-. It should be noted that the reduction potentials of the closed form of the dyes were outside the electrochemical window of the analytical solvent, preventing their direct measurement. Therefore, the experimental LUMO values were estimated from the HOMO energy levels and the band gap obtained by UV-visible spectroscopy. The LUMO levels of the colored isomers of the dyes are strongly shifted to lower values and are all in the same range, ranging from −3.9 eV to −3.8 eV. According to the theoretical calculation, in the uncolored isomers, the LUMO is highly localized on the cyano-acrylic acid acceptor unit. However, once the molecule is opened, the LUMO is spatially delocalized to the diene system and the carbonyl unit. The LUMO levels of **SF1-5** are comparable to **NP2** as expected since the dyes are designed with the same electron-accepting units.

The effects induced by the unsubstituted and substituted carbazoles are more pronounced when looking at the HOMO levels. First, it can be seen that when carbazoles are functionalized with diphenylamine units, the HOMO level is around −5.2 eV and −5 eV as for **NP2**. Without diphenylamine, the carbazole units allow the HOMO level to be lowered to −5.4 eV and up to −5.5 eV. This feature is particularly interesting as it opens the way for the use of alternative redox couples to triiodide/iodide system, such as cobalt-based complexes, which has a higher redox potential. It is also important to note that for the closed isomers, the HOMO is completely localized on the carbazole units when they are functionalized, but tends to extend into the core of the molecule for the unsubstituted carbazole. For open isomers, the HOMO is partially delocalized on the indeno unit, except when diphenylamines are used as substituents.

Photovoltaic performances in opaque dye-sensitized solar cells

To evaluate the photovoltaic performance of the new photochromes, we fabricated opaque DSSCs. For comparison purposes, we tested all the dyes in the same device

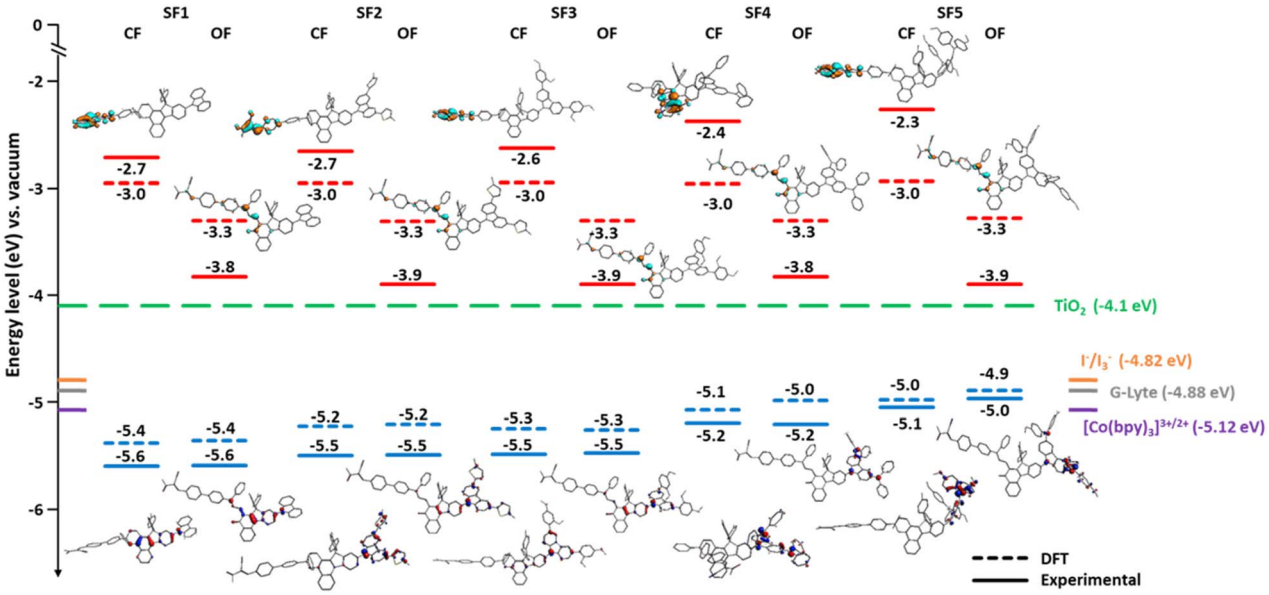

Fig. 3 Energy band diagram and electron density distributions on the dyes. Experimental- and DFT-calculated energy levels of the frontier orbitals of the dyes and their spatial localizations (closed- (CF) and open-form (OF) trans-isomers). LUMO energy levels are shown in cyan and orange and HOMO energy levels are shown in blue and red (all *versus* the vacuum level). The positions of the conduction band edge (CB) of TiO2 and the Nernst potential of the tri-iodide/iodide redox couple are indicated with horizontal dashed lines (green and orange, respectively).[41,49,50] Cyclic voltammetries (CV) were performed at a concentration of 2×10^{-3} mol L^{-1} in DCM, Ag/Ag^{+} reference, Pt electrode, Fc^{+}/Fc internal reference. DFT modeling: B3LYP hybrid functional + dispersion and TZ2P basis sets in a COSMO model for DCM.

configuration and compared them with **NP2** as a reference dye. The evaluation of photochromic DSSCs requires the recording of the current–voltage characteristics at different time intervals of light exposure (standard AM1.5G irradiation at 1000 W m^{-2}) until the cells reach the PSS (see Fig. 4). Once the cells have reached the PSS corresponding to the stabilisation of the short-circuit current density (J_{SC}), we measure the open-circuit voltage (V_{OC}), the fill factor (FF) and thus the PCE. Further experimental details on the fabrication and characterization of the solar cells are given in the ESI.†

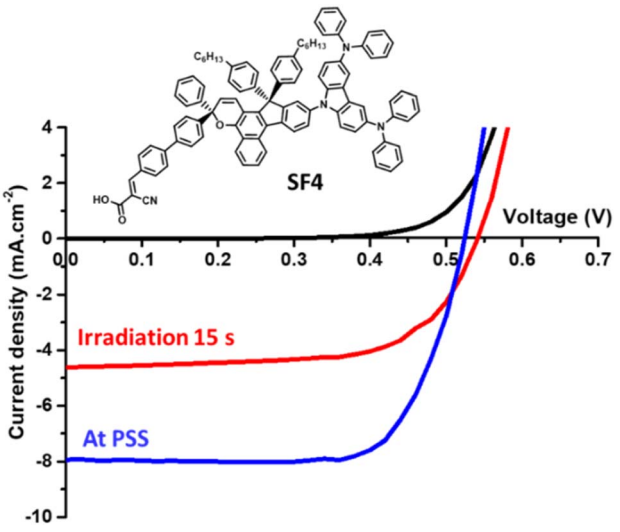

Fig. 4 *J*–*V* curves of a **SF4**-based opaque photochromic solar cell registered in the dark (black line), after 15 seconds under irradiation (red line) and at PSS reached after 300 seconds under continuous irradiation (blue line). Standard irradiation conditions were AM 1.5 G, 1000 W × m^{-2} at 25 °C.

We tested the dyes with and without chenodeoxycholic acid (CDCA), a co-adsorbent that helps to reduce aggregate formation[51,52] and increase V_{OC}.[53] We found that the use of CDCA had little effect on the performance of the devices, which was however slightly improved when it was used at a Dye/CDCA ratio of 1 : 10. Table 2 summarizes the performance obtained with the dyes. The study of the dyes in DSSCs shows quite different behaviors depending on the carbazole unit employed. Firstly, they are all less efficient than **NP2** and this is mainly related to the lower J_{SC} generated with the new dyes despite comparable dye loading in some cases. This could be explained by their lower absorption in the visible region.

SF1 has the poorest photovoltaic performance, due to a low J_{SC} of around 2.5 mA cm^{-2}, although the dye loading is highest with this dye.

As the size of the donor group increases, the amount of dye attached to the surface decreases, but this has no negative influence on the J_{SC}. **SF2** and **SF3** have very similar efficiencies but different photovoltaic parameters. **SF2** gives a higher J_{SC}, while **SF3** gives a higher V_{OC} and FF. Then, although the two dyes have the lowest colourability (see Table 1), **SF4** and **SF5** show the highest photogenerated current with a J_{SC} of 7.93 mA cm^{-2} and 6.01 mA cm^{-2}, respectively. Due to better V_{OC} and FF, **SF4** has the best performance among the five new dyes, with a PCE of 3.04%. For this class of dyes, where the photovoltaic performance depends not only on the optoelectronic properties of the dyes but also on the photochromic behavior, it seems

Table 2 Photovoltaic parameters of the solar cells fabricated with opaque (13 μm mesoporous + 3 μm scattering layer) electrodes from the same batch under irradiation AM1.5G at 1000 W × m^{-2}. The dye: CDCA molar ratio was set to 1 : 10 for comparison purposes (except for **NP2**), dye: CDCA molar ratio was set to 1 : 5. Statistical data was obtained for at least 3 cells. For the dye loading the mean value and standard deviations (in parenthesis) are also given for 3 cells

Dye	J_{SC} (mA cm^{-2})	V_{OC} (mV)	FF	PCE (%)	Dye loading (mol cm^{-2}) × 10^{-8}
NP2	12.74 (13.55 ± 0.67)	503 (491 ± 1)	0.649 (0.620 ± 0.020)	4.16 (4.12 ± 0.04)	21.5
SF1	2.78 (2.50 ± 0.37)	482 (491 ± 11)	0.667 (0.674 ± 0.007)	0.89 (0.82 ± 0.10)	18 (±3.5)
SF2	5.24 (4.78 ± 0.55)	474 (488 ± 16)	0.672 (0.683 ± 0.015)	1.67 (1.59 ± 0.11)	14 (±3.8)
SF3	4.36 (4.20 ± 0.14)	527 (528 ± 15)	0.720 (0.724 ± 0.007)	1.65 (1.61 ± 0.06)	8 (±4.9)
SF4	7.93 (7.92 ± 0.13)	524 (523 ± 2)	0.731 (0.720 ± 0.010)	3.04 (2.98 ± 0.07)	10 (±9.5)
SF5	6.01 (6.10 ± 0.10)	468 (469 ± 1)	0.512 (0.494 ± 0.018)	1.44 (1.41 ± 0.03)	7 (±10)

difficult to establish clear structure–property relationships by analyzing the photovoltaic parameter alone. In order to better understand the photochromic behavior of the carbazole dyes in DSSCs and their influence on recombination processes, electrochemical impedance spectroscopy (EIS) was performed.

Electrochemical impedance spectroscopy (EIS)

EIS measurements were performed under red illumination (655 nm) to avoid unwanted activation of the photochromic molecules.[54] The devices were measured before and after applying 15 minutes of continuous light exposure under 1 Sun, to ensure that the PSS was reached.[25] The resulting Nyquist plots are shown in Fig. 5. For the five different dyes, the Nyquist plot show two well-defined semi-circles with different time constants.[55,56] At high frequencies, the first point corresponds to the series resistance (R_S), which takes into account for the external elements of the circuit, such as wiring, contacts and experimental setup.[57] This is followed by a small semicircle that does not depend exponentially on the light intensity, which can be linked to reactions in the cathode,[55,56] but is beyond the scope of this work. The second arc, which varies with light intensity, is the most relevant in this case, because it is the result of the parallel combination of the interfacial recombination resistance (R_{rec}) associated with the chemical capacitance of electron accumulation in the semiconductor film (C_μ).[58–60]

Both semicircles are connected by a 45° Warburg line diffusion element, which is related to the electron transport resistance in the TiO_2[59]. These impedance spectra were fitted using the transmission line equivalent circuit.[59,61] For all photochromic dyes in this family except **SF3** and **SF5**, the recombination semicircle shrinks after light irradiation. This means that the isomerization of the dye molecules creates additional recombination paths, as has already been described for other photochromic dyes.[25,36,54] On the other hand, for **SF3** and **SF5** the isomerization of the dyes reduces the recombination, suggesting that the introduction of four alkoxy chains in the donor part of the dye protects the devices against the local I_3^- concentration increase at the surface of the metal oxide.

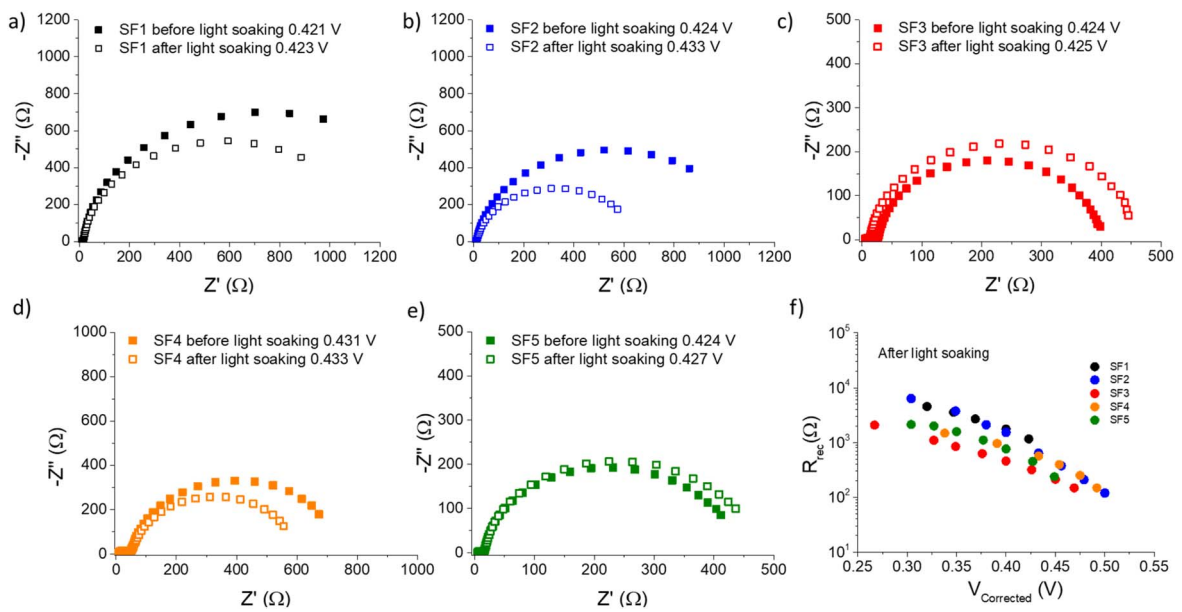

Fig. 5 (a–e) Electrochemical impedance spectroscopy results of **SF1-5** dyes solar cells. The Nyquist plots are shown both before and after light soaking. (f) Recombination resistance *vs.* corrected voltage for **SF1-5** dyes under red illumination and after light soaking. Note: the comparison of the recombination resistance *vs.* corrected voltage for **SF1-5** dyes before and after light soaking, can be found in ESI.†

This result is consistent with observations usually made on the classical dyes used in DSSCs. Both, R_{rec} and C_μ are known to have a voltage dependence.[62,63] This exponential dependence can be expressed as follows:

$$C_\mu = C_0 \exp\left(\frac{\alpha q V_{oc}}{k_B T}\right) \quad (1)$$

$$R_{rec} = R_0 \exp\left(-\frac{\beta q V}{k_B T}\right) \quad (2)$$

where C_0[64,65] and R_0[61] are numerical pre-factors, α[62,66] is the trap distribution parameter related to the average depth of the trap states which determines the CB alignment, β[67] is the recombination reaction order, k_B is the Boltzmann constant and T is the absolute temperature. As it can be seen in Table S1 (ESI†), the values of α and β are within the normal values reported for DSSCs[66–68] (0.15–0.35 for α and 0.5–0.8 for β) except for **SF3** and **SF5**, where β is slightly below this threshold. Fig. S2 (ESI†) shows the resulting capacitances from of the impedance spectrum fitting. No significant band shift is observed between the closed and open forms of the different dyes. However, **SF3** shows a band shift of 50 mV compared to the other dyes. This means that a voltage correction must be made to ensure that the comparison of the recombination resistances is made at the same electron density at the photoanode,[61,65,69] thus distinguishing thermodynamics from kinetics[70,71] (Fig. 5). As it can be seen in Fig. 5, **SF2** and **SF4** show the highest values of recombination resistance at high light intensities. Comparing the impedance results with the V_{OC} shown in Table 2, the high value of **SF3** can be related to the presence of the band shift while the increase in the V_{OC} for **SF4** is due to a higher protection against recombination. Looking at the molecular structure of the **SF3** and **SF5** dyes, one would expect a passivation of the recombination due to the introduction of the four alkoxy chains. However, this phenomenon is not observed in Fig. 5. These results, together with the anomalous β-values reported in Table S1 (ESI†), suggest that recombination with I_3^- species decreases; the dye regeneration would be slower, so that the oxidised dye molecules act as an additional recombination pathway.

Semi-transparent photochromic solar cells with high color-rendering index

One of the main advantages of using photochromic dyes in semi-transparent solar cells is their ability to change their absorption spectrum under irradiation and thus modulating the light transmitted through the device. They are of particular interest for the development of multifunctional solar cells whose light transmittance and current generation can self-adapt to sunlight conditions. In the next part of this work, we focus on the fabrication of semi-transparent cells based on **SF4**, as this dye was found to be the most efficient in opaque solar cells. For the development of semi-transparent solar cells that can be used as glazing in the future, it is important for user comfort that the cells have good transparency level in the visible range, but also a high CRI. The CRI is a quantitative measure of the ability of a light source to accurately reproduce the colours of an object compared to a natural or standard light source.[72] To calculate the AVT of the cells we used the formula reported by Griffoni *et al.*:[73]

$$AVT(\%) = \frac{\int T(\lambda) V(\lambda) S(\lambda) d(\lambda)}{\int V(\lambda) S(\lambda) d(\lambda)}$$

where, λ is the wavelength, T is the transmittance, V is the photopic response and S is the solar photon flux (AM1.5G).

To determine the CRI of the semi-transparent devices, we developed a Python code to calculate the spectrum of the sun (AM1.5G) through the solar cells to consider the sun-cell combination as a light source. We then used the colour science library[74] to determine not only the overall CRI value but also the detailed CRI for each colour and the coordinates in the chromaticity diagram (CIE 1931 colour space). The Python code is described and available in ESI.† For the fabrication of the solar cells, we used 9μm-thick transparent electrodes and different electrolytes containing different redox mediators with different transparency in the visible range with the aim of improving the CRI of the cells. Three electrolytes were tested, the first two ones being home-made electrolytes based on iodine and cobalt-based redox couples[75,76] and the last one being an acetonitrile sulfurothiolate/iodide hybrid electrolyte,[77] commercialized by G-Lyte. From the performances reported in Table 3, it can be seen that the cells containing the iodine or mixed sulfurothioate/iodide electrolytes show the best performances with a PCE above 2.1%, which is mainly due to current densities above 6.5 mA cm^{-2}.

The solar cells with the cobalt-based electrolyte showed lower performances associated with a lower J_{SC}. This can be explained by the slower diffusion of Co^{2+} in the mesopores than that of I^-. It should be noted that the mesoporous electrodes used with the three electrolytes are identical and that the pore size has not been adapted to cobalt complexes,[78] which are large redox species.

If we now look at the optical properties of these devices, we see that the cells before activation have quite high transparency in the visible range, on average around 55%. It should be noted here that the electrodes are relatively thick and that we did not use anti-reflective coatings to minimize the glass reflection. After activating the cells by exposing them to light for 10 minutes, the AVT drops to values comprised between 20% and 26%, with the more transparent devices being those made with cobalt-based electrolytes. What is most interesting is that cells made with **SF4** have very high CRIs before activation, between 91.8 and 95.5 and after activation they maintain CRI values between 82.1 and 87 on average. The type of the electrolyte seems to have a little influence on the CRI although the best values are obtained with the electrolyte containing cobalt. The coloration process of the photochromic solar cells is fully reversible and the initial transparency is completely recovered after a few hours in the dark.

To demonstrate the potential of the new dye for the fabrication of larger area devices, we fabricated a 23 cm^2 semi-

Table 3 Photovoltaic and optical properties of transparent solar cells sensitized with **SF4**. Cell fabrication: TiO2 0.36 cm^2, 9 μm thickness, transparent, purchased from Solaronix. Dyeing bath: **SF4** 0.5 mmol L^{-1} and CDCA 5 mmol L^{-1} in CHCl3/tBuOH 1/1. Iodine electrolyte: I_2 90 mmol L^{-1}, LiI 0.5 mol L^{-1} in ACN. Cobalt electrolyte: 0.22 mol L^{-1} $Co(bpy)_3(PF_6)_2$ + 0.05 mol L^{-1} $Co(bpy)_3(PF_6)_3$ in ACN. G-lyte electrolyte provided by the company. Best cells and average of two cells in parenthesis

	Photovoltaic performances				Optical properties			
SF4	J_{SC} (mA cm^{-2})	V_{OC} (mV)	FF	PCE (%)	AVT CF (%)	CRI CF	AVT OF (%)	CRI OF
Iodine	6.86 (6.44)	518 (529)	0.651 (0.656)	2.31 (2.23)	55.3 (55.6)	91.8 (91.8)	24.2 (24.1)	86.2 (86.1)
Cobalt	3.68 (3.81)	532 (528)	0.675 (0.607)	1.32 (1.22)	54.3 (55.5)	95.7 (95.5)	26.0 (24.9)	88.2 (87.0)
G-Lyte	7.48 (6.72)	456 (479)	0.644 (0.674)	2.20 (2.15)	54.6 (55.2)	94.7 (94.1)	20.5 (20.6)	81.6 (82.1)

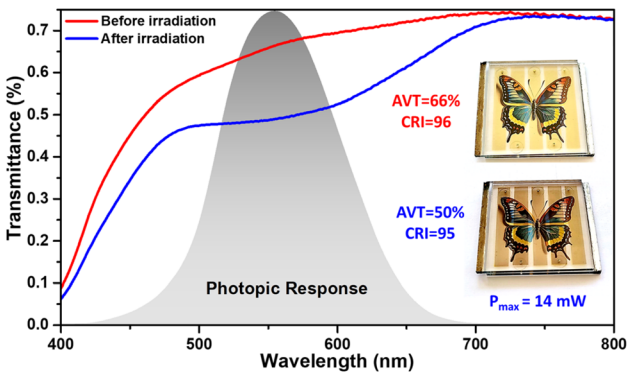

Fig. 6 Visible-light transmittance of a solar cell comprised in a semi-transparent mini-module and spectrum of the photopic response of the human eye for comparison. Picture of a colored butterfly taken through the mini-module (total area: 23 cm^2) in the non-activated state (top) and activated state (bottom). The power output was measured under 1 Sun (1000 W m^{-2}).

transparent mini-module with an active area of 14.08 cm^2, corresponding to about 61% of the total area. The mini-module contains 5 rectangular cells connected in series following in a W-type design.

In order to optimize the transparency in the visible, the thickness of the mesoporous layer was fixed at around 7 μm without using a scattering layer, the platinum catalyst used as counter-electrode was sprayed and the G-Lyte electrolyte was chosen as it gives the highest J_{SC} in transparent solar cells. Before exposure to sunlight, the colored parts of the device have an AVT of 66% and display a bright yellow-beige color with a CRI of 96. After activation under light (1 Sun) for 60 seconds on each side, the colored parts of the device turn brown and their AVT drops to 50% while maintaining an excellent CRI of 95 (see Fig. 6). At the same time, the photovoltaic parameters increase and the device reaches a maximum power output of 14 mW. These results clearly show that thanks to these dyes, it is possible to design semi-transparent photovoltaic devices that guarantee comfortable vision with good color perception regardless of the activation state of the cells. The coloring of these devices is fast and takes only a few minutes (See film in ESI†).

Conclusion

In conclusion, we have proposed a simple method based on the molecular engineering of push–pull photochromic dyes to obtain photosensitizers whose absorption spectrum in the activated state coincides with the photopic response of the human eye. We report the synthesis of five new molecules with a Donor-Pi-Acceptor structure in which the photochromic core is a diphenyl-naphthopyran moiety and the electron donor moiety is a carbazole derivative. We show that, in the activated state, these molecules have a blue-shifted absorption compared to an analogue molecule based on a diphenylamine unit. The coloured isomers of these photochromic dyes have an absorption spectrum with a maximum comprised between 546 nm and 571 nm in solution and they exhibit a rather rapid discoloration kinetics. When used as photosensitizers in DSSCs, the dyes retain their photochromic properties and achieve efficiencies of above 3% in opaque cells and 2.2% in transparent cells. In this study, we report for the first time the use of electrolytes with alternative redox systems to iodine with this class of dyes. We have fabricated semi-transparent solar cells with self-adapting optical transmission and showing light-induced transparency variations of 25–30%.

Finally, using one of these dyes, we demonstrate the fabrication of a semi-transparent solar mini-module (with an active area of 14.08 cm^2), giving a power output of 14 mW. The mini-module shows excellent CRI values in both the non-activated and activated states, exceeding 95. These results demonstrate that molecular engineering of photochromic sensitizers is a relevant strategy for the development of semi-transparent solar cells with dynamic optical properties. We show that translucent solar cells capable of changing colour and having self-adjusting transparency to light conditions can be designed while providing visual comfort to users.

Data availability

The ESI† contains all experimental details, including the synthetic method, characterization of all chemical products reported in this study. NMR spectra of all compounds are included. The Python program developed and used in this work is available on GitHub. **https://github.com/Samuel-Fauvel/CRI-AVT-Solar-Cells**; (DOI: **https://10.5281/zenodo.8189369**). The raw data for Fig. 2 (optical properties), Fig. 4 (*J*–*V* curves for best cells and statistical analysis), Fig. 6 (*I*–*V* and *P*–*V* curves for the mini-module and transmittance for activated and non-activated mini-module), DFT and TD-DFT files, are available at Open Science Framework, **https://osf.io/tvrxy/**, (DOI: **https://10.17605/OSF.IO/TVRXY**).

Author contributions

S. F., J. M. A. C., Y. K. synthesized and characterized the molecules (investigation-methodology-visualization). S. F., A. J. R., V. M. M, S. N. fabricated and characterized the solar cells. V. M. M. and A. J. R. performed the EIS measurements (investigation-methodology-visualization). V. C and F. S. developed the G-Lyte electrolyte. P. M. and S. F. performed the DFT calculation. S. F. developed the python program used in this work. C. A. co-supervised the work and analyzed the data (supervision-validation). R. D. acquired the financial support, led the research activity, designed the materials and experiments, supervised the work, cured the data and wrote the manuscript (conceptualization-funding acquisition-analysis-methodology-supervision-validation-writing-editing). All authors contributed to the work and gave approval to the final version of the manuscript.

Conflicts of interest

The authors declare no conflict of interest.

Acknowledgements

F. S. thanks Dr W. Naim and Dr F. Grifoni for the help in the development of the G-Lyte electrolyte. R. D. thanks Dr J. Liotier for his help during the synthesis of some of the precursors. P. M. thanks GENCI (CINES and IDRIS) for high-performance computing resources (grant 2019-A0060807648). R. D. acknowledges the European Research Council (ERC) for funding. This work was funded under the European Union's Horizon 2020 research and innovation programme (grant agreement number 832606; project PISCO).

Notes and references

1 S. A. Hashemi, S. Ramakrishna and A. G. Aberle, *Energy Environ. Sci.*, 2020, **13**, 685–743.
2 A. Fakharuddin, R. Jose, T. M. Brown, F. Fabregat-Santiago and J. Bisquert, *Energy Env. Sci*, 2014, **7**, 3952–3981.
3 D. Luo, W. Jang, D. D. Babu, M. S. Kim, D. H. Wang and A. K. K. Kyaw, *J. Mater. Chem. A*, 2022, **10**, 3255–3295.
4 A. S. R. Bati, Y. L. Zhong, P. L. Burn, M. K. Nazeeruddin, P. E. Shaw and M. Batmunkh, *Commun. Mater.*, 2023, **4**, 1–24.
5 K. Khandelwal, S. Biswas, A. Mishra and G. D. Sharma, *J. Mater. Chem. C*, 2021, **10**, 13–43.
6 S. Dai and X. Zhan, *Adv. Energy Mater.*, 2018, **8**, 1800002.
7 A. B. Muñoz-García, I. Benesperi, G. Boschloo, J. J. Concepcion, J. H. Delcamp, E. A. Gibson, G. J. Meyer, M. Pavone, H. Pettersson, A. Hagfeldt and M. Freitag, *Chem. Soc. Rev.*, 2021, **50**, 12450–12550.
8 R. Haridas, J. Velore, S. C. Pradhan, A. Vindhyasarumi, K. Yoosaf, S. Soman, K. N. N. Unni and A. Ajayaghosh, *Mater. Adv.*, 2021, **2**, 7773–7787.
9 D. B. Ritzer, B. A. Nejand, M. A. Ruiz-Preciado, S. Gharibzadeh, H. Hu, A. Diercks, T. Feeney, B. S. Richards, T. Abzieher and U. W. Paetzold, *Energy Environ. Sci.*, 2023, **16**, 2212–2225.
10 S. Yoon, S. Tak, J. Kim, Y. Jun, K. Kang and J. Park, *Build. Environ.*, 2011, **46**, 1899–1904.
11 A. Cannavale, G. E. Eperon, P. Cossari, A. Abate, H. J. Snaith and G. Gigli, *Energy Environ. Sci.*, 2015, **8**, 1578–1584.
12 H. M. Lee and J. H. Yoon, *Appl. Energy*, 2018, **225**, 1013–1021.
13 B. Commault, T. Duigou, V. Maneval, J. Gaume, F. Chabuel and E. Voroshazi, *Appl. Sci.*, 2021, **11**, 11598.
14 A. Dessì, D. A. Chalkias, S. Bilancia, A. Sinicropi, M. Calamante, A. Mordini, A. Karavioti, E. Stathatos, L. Zani and G. Reginato, *Sustain. Energy Fuels*, 2021, **5**, 1171–1183.
15 D. A. Chalkias, C. Charalampopoulos, A. K. Andreopoulou, A. Karavioti and E. Stathatos, *J. Power Sources*, 2021, **496**, 229842.
16 A. Hagfeldt, G. Boschloo, L. Sun, L. Kloo and H. Pettersson, *Chem. Rev.*, 2010, **110**, 6595–6663.
17 Y. Ren, D. Zhang, J. Suo, Y. Cao, F. T. Eickemeyer, N. Vlachopoulos, S. M. Zakeeruddin, A. Hagfeldt and M. Grätzel, *Nature*, 2023, **613**, 60–65.
18 H. Michaels, M. Rinderle, I. Benesperi, R. Freitag, A. Gagliardi and M. Freitag, *Chem. Sci.*, 2023, **14**, 5350–5360.
19 D. Joly, L. Pellejà, S. Narbey, F. Oswald, J. Chiron, J. N. Clifford, E. Palomares and R. Demadrille, *Sci. Rep.*, 2014, **4**, 4033.
20 N. Kato, H. Tanaka, Y. Takeda, K. Higuchi and J. Nakajima, *ACS Sustain. Chem. Eng.*, 2023, **11**, 5014–5022.
21 R. Escalante, D. Pourjafari, D. Reyes-Coronado and G. Oskam, *J. Renew. Sustain. Energy*, 2016, **8**, 023704.
22 C. A. Gonzalez-Flores, D. Pourjafari, R. Escalante, E. J. Canto-Aguilar, A. V. Poot, J. M. Andres Castán, Y. Kervella, R. Demadrille, A. J. Riquelme, J. A. Anta and G. Oskam, *ACS Appl Energy Mater*, 2022, **5**, 14092–14106.
23 L. Vesce, P. Mariani, M. Calamante, A. Dessì, A. Mordini, L. Zani and A. Di Carlo, *Sol. RRL*, 2022, **6**, 2200403.
24 N. Mariotti, M. Bonomo, L. Fagiolari, N. Barbero, C. Gerbaldi, F. Bella and C. Barolo, *Green Chem.*, 2020, **22**, 7168–7218.
25 Q. Huaulmé, V. M. Mwalukuku, D. Joly, J. Liotier, Y. Kervella, P. Maldivi, S. Narbey, F. Oswald, A. J. Riquelme, J. A. Anta and R. Demadrille, *Nat. Energy*, 2020, **5**, 468–477.
26 G. Berkovic, V. Krongauz and V. Weiss, *Chem. Rev.*, 2000, **100**, 1741–1754.
27 M. Irie, T. Fukaminato, K. Matsuda and S. Kobatake, *Chem. Rev.*, 2014, **114**, 12174–12277.
28 Y. Zhuge, D. Xu, C. Zheng and S. Pu, *Anal. Chim. Acta*, 2019, **1079**, 153–163.
29 M. Qin, Y. Huang, F. Li and Y. Song, *J. Mater. Chem. C*, 2015, **3**, 9265–9275.
30 R. A. Evans, T. L. Hanley, M. A. Skidmore, T. P. Davis, G. K. Such, L. H. Yee, G. E. Ball and D. A. Lewis, *Nat. Mater.*, 2005, **4**, 249–253.
31 D. Kim, K. Jeong, J. E. Kwon, H. Park, S. Lee, S. Kim and S. Y. Park, *Nat. Commun.*, 2019, **10**, 3089.
32 Y. Xiong, A. V. Jentzsch, J. W. M. Osterrieth, E. Sezgin, I. V. Sazanovich, K. Reglinski, S. Galiani, A. W. Parker,

C. Eggeling and H. L. Anderson, *Chem. Sci.*, 2018, **9**, 3029–3040.
33 Z. Zhou, W. Yuan and X. Xie, *Mater. Chem. Front.*, 2022, **6**, 3359–3368.
34 W. Wu, J. Wang, Z. Zheng, Y. Hu, J. Jin, Q. Zhang and J. Hua, *Sci. Rep.*, 2015, **5**, 8592.
35 N. M. Johnson, Y. Y. Smolin, C. Shindler, D. Hagaman, M. Soroush, K. K. S. Lau, H.-F. Ji, N. M. Johnson, Y. Y. Smolin, C. Shindler, D. Hagaman, M. Soroush, K. K. S. Lau and H.-F. Ji, *AIMS Mater. Sci.*, 2015, **2**, 503–509.
36 V. M. Mwalukuku, J. Liotier, A. J. Riquelme, Y. Kervella, Q. Huaulmé, A. Haurez, S. Narbey, J. A. Anta and R. Demadrille, *Adv. Energy Mater.*, 2023, **13**, 2203651.
37 A. Ghosh, P. Selvaraj, S. Sundaram and T. K. Mallick, *Sol. Energy*, 2018, **163**, 537–544.
38 C. Yang, D. Liu, M. Bates, M. C. Barr and R. R. Lunt, *Joule*, 2019, **3**, 1803–1809.
39 A. Venkateswararao, K. R. J. Thomas, C.-P. Lee, C.-T. Li and K.-C. Ho, *ACS Appl. Mater. Interfaces*, 2014, **6**, 2528–2539.
40 P. Naik, A. Planchat, Y. Pellegrin, F. Odobel and A. Vasudeva Adhikari, *Sol. Energy*, 2017, **157**, 1064–1073.
41 W. Naim, F. Grifoni, V. Challuri, D. Mathiron, S. Ceurstemont, P. Chotard, T. Alnasser, I. Dzeba, N. Barbero, S. Pilard, C. Barolo and F. Sauvage, *Cell Rep. Phys. Sci.*, 2023, 101455.
42 Ikamba organics, **https://ikambalab.com/**, accessed 26 April 2023.
43 P. J. Coelho, L. M. Carvalho, A. M. C. Fonseca and M. M. M. Raposo, *Tetrahedron Lett.*, 2006, **47**, 3711–3714.
44 R. Demadrille, A. Rabourdin, M. Campredon and G. Giusti, *J. Photochem. Photobiol. Chem.*, 2004, **168**, 143–152.
45 H. Bouas-Laurent, *Photochromism: molecules and systems*, Elsevier; Distributors for the U.S. and Canada, Elsevier Science Pub. Co, Amsterdam, New York, New YorK, NY, U.S.A, 1990.
46 M. J. Robb, T. A. Kim, A. J. Halmes, S. R. White, N. R. Sottos and J. S. Moore, *J. Am. Chem. Soc.*, 2016, **138**, 12328–12331.
47 J. Liotier, V. M. Mwalukuku, S. Fauvel, A. J. Riquelme, J. A. Anta, P. Maldivi and R. Demadrille, *Sol. RRL*, 2022, **6**, 2100929.
48 J. Momoda, S. Izumi and Y. Yokoyama, *Dyes Pigments*, 2015, **119**, 95–107.
49 T. W. Hamann, *Dalton Trans.*, 2012, **41**, 3111–3115.
50 V. V. Pavlishchuk and A. W. Addison, *Inorganica Chim. Acta*, 2000, **298**, 97–102.
51 L. Zhang and J. M. Cole, *ACS Appl. Mater. Interfaces*, 2015, **7**, 3427–3455.
52 L. Zhang and J. M. Cole, *J. Mater. Chem. A*, 2017, **5**, 19541–19559.
53 L. Mao, S. Dun, H. Ren, J. Jiang, X. Guo, F. Huang, P. Heng, L. Wang, J. Zhang and H. Ågren, *J. Mater. Chem. C*, 2021, **9**, 5800–5807.
54 A. J. Riquelme, V. M. Mwalukuku, P. Sánchez-Fernández, J. Liotier, R. Escalante, G. Oskam, R. Demadrille and J. A. Anta, *ACS Appl Energy Mater*, 2021, **4**, 8941–8952.
55 J. Idígoras, E. Guillén, F. J. Ramos, J. A. Anta, M. K. Nazeeruddin and S. Ahmad, *J. Mater. Chem. A*, 2014, **2**, 3175–3181.
56 A. Hauch and A. Georg, *Electrochim. Acta*, 2001, **46**, 3457–3466.
57 E. von Hauff, *J. Phys. Chem. C*, 2019, **123**, 11329–11346.
58 Q. Wang, J.-E. Moser and M. Grätzel, *J. Phys. Chem. B*, 2005, **109**, 14945–14953.
59 J. Bisquert, *J. Phys. Chem. B*, 2002, **106**, 325–333.
60 J. Bisquert, I. Mora-Sero and F. Fabregat-Santiago, *ChemElectroChem*, 2014, **1**, 289–296.
61 F. Fabregat-Santiago, G. Garcia-Belmonte, I. Mora-Seró and J. Bisquert, *Phys. Chem. Chem. Phys.*, 2011, **13**, 9083–9118.
62 J. Bisquert, *Phys. Chem. Chem. Phys.*, 2003, **5**, 5360–5364.
63 J. A. Anta, J. Idígoras, E. Guillén, J. Villanueva-Cab, H. J. Mandujano-Ramírez, G. Oskam, L. Pellejà and E. Palomares, *Phys. Chem. Chem. Phys.*, 2012, **14**, 10285–10299.
64 S. R. Raga, E. M. Barea and F. Fabregat-Santiago, *J. Phys. Chem. Lett.*, 2012, **3**, 1629–1634.
65 D. Pourjafari, D. Reyes-Coronado, A. Vega-Poot, R. Escalante, D. Kirkconnell-Reyes, R. García-Rodríguez, J. A. Anta and G. Oskam, *J. Phys. Chem. C*, 2018, **122**, 14277–14288.
66 J. R. Jennings, A. Ghicov, L. M. Peter, P. Schmuki and A. B. Walker, *J. Am. Ceram. Soc.*, 2008, **130**, 13364–13372.
67 J. Bisquert and I. Mora-Seró, *J. Phys. Chem. Lett.*, 2010, **1**, 450–456.
68 J. Bisquert, A. Zaban and P. Salvador, *J. Phys. Chem. B*, 2002, **106**, 8774–8782.
69 L. M. Peter, *J. Phys. Chem. C*, 2007, **111**, 6601–6612.
70 R. Kern, R. Sastrawan, J. Ferber, R. Stangl and J. Luther, *Electrochim. Acta*, 2002, **47**, 4213–4225.
71 J. Manuel Vicent-Luna, J. Idigoras, S. Hamad, S. Calero and J. Antonio Anta, *J. Phys. Chem. C*, 2014, **118**, 28448–28455.
72 H. Meddeb, M. Götz-Köhler, N. Neugebohrn, U. Banik, N. Osterthun, O. Sergeev, D. Berends, C. Lattyak, K. Gehrke and M. Vehse, *Adv. Energy Mater.*, 2022, **12**, 2200713.
73 F. Grifoni, M. Bonomo, W. Naim, N. Barbero, T. Alnasser, I. Dzeba, M. Giordano, A. Tsaturyan, M. Urbani, T. Torres, C. Barolo and F. Sauvage, *Adv. Energy Mater.*, 2021, **11**, 2101598.
74 C. Developers, *Colour Science for Python*, **https://www.colour-science.org/**, accessed 26 April 2023.
75 H. N. Tsao, C. Yi, T. Moehl, J.-H. Yum, S. M. Zakeeruddin, M. K. Nazeeruddin and M. Grätzel, *ChemSusChem*, 2011, **4**, 591–594.
76 J.-H. Yum, E. Baranoff, F. Kessler, T. Moehl, S. Ahmad, T. Bessho, A. Marchioro, E. Ghadiri, J.-E. Moser, C. Yi, M. K. Nazeeruddin and M. Grätzel, *Nat. Commun.*, 2012, **3**, 631.
77 T. Baron, W. Naim, I. Nikolinakos, B. Andrin, Y. Pellegrin, D. Jacquemin, S. Haacke, F. Sauvage and F. Odobel, *Angew. Chem., Int. Ed.*, 2022, **61**, e202207459.
78 A. Yella, S. Mathew, S. Aghazada, P. Comte, M. Grätzel and M. K. Nazeeruddin, *J. Mater. Chem. C*, 2017, **5**, 2833–2843.